ACS APPLIED MATERIALS & INTERFACES

Research Article

www.acsami.org

Facile Preparation of Water-Dispersible Graphene Sheets Stabilized by Carboxylated Oligoanilines and Their Anticorrosion Coatings

Lin Gu, Shuan Liu,* Haichao Zhao,* and Haibin Yu

Key Laboratory of Marine Materials and Related Technologies, Zhejiang Key Laboratory of Marine Materials and Protective Technologies, Ningbo Institute of Materials Technology and Engineering, Chinese Academy of Sciences, Ningbo 315201, P. R. China

Supporting Information

ABSTRACT: Dispersion of graphene in solvents is of crucial importance toward its practical applications. In this study, using a water-soluble carboxylated aniline trimer derivative (CAT^-) as a stabilizer, the commercial graphene can be stably dispersed in water at high concentration (>1 mg/mL) via strong $\pi-\pi$ interaction that was proved by Raman and UV−vis spectra. Moreover, the CAT^--functionalized graphene sheets (G-CAT^- hybrid) exhibited high conductivity (~1.5 S/cm), good electroactivity and improved electrochemical stability. The addition of well-dispersed graphene into waterborne epoxy system (G-CAT^-/epoxy) remarkably improved corrosion protection compared with pure waterborne epoxy coating, based on a series of electrochemical measurements performed under 3.5% NaCl solution. This significantly enhanced anticorrosion performance is mainly due to the improved water barrier properties derived from highly dispersed graphene nanosheets in the epoxy coating.

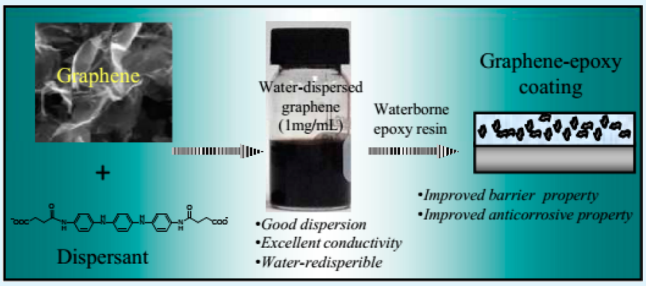

KEYWORDS: *graphene, carboxylated oligoaniline, dispersion, electroactivity, anticorrosion*

1. INTRODUCTION

Graphene as a 2D layer of sp^2-hybridization carbon has drawn a great deal of attention because it has remarkable thermal, mechanical, electrical, and barrier properties, and promising applications in microelectrical devices,[1] nanocomposites,[2] hydrogen storage,[3] metal protection,[4] and so on. Large-scale preparation of graphene powder has been realized by the chemical reduction of exfoliated graphene oxide (GO)[5] or the liquid-phase exfoliation from natural graphite.[6] However, because of its strong van der Waals forces and high specific surface area, graphene easily aggregates together, which greatly limits its further processing.[7,8] Therefore, the availability of large quantities of dispersible graphenes is a prerequisite for the further development of most proposed applications.

Generally, chemical modifications and noncovalent functionalizations have been employed to prepare water-soluble or dispersible graphene sheets.[9] For the former methods, water-soluble graphene can be obtained by grafting specific hydrophilic groups such as carboxylic and sulfonate groups on its basal planes.[10,11] Nevertheless, the grafting modification involves tedious chemical routes and tends to induce defects in graphene, which alters its intrinsic thermal conductivity and electrical properties.[12] In contrast, noncovalent functionalization is considered to be a promising method becaseu of its high efficiency, ease of control, and higher conservation of graphene's properties.[13,14] The reduction of graphene oxide in the present of water-soluble small molecules or polymers, such as pyrenebutyric acid derivative,[15] sulfonated polyaniline,[13] poly(sodium 4-styrenesulfonate),[16] can form a stable aqueous dispersion of graphene sheets, based on $\pi-\pi$ interactions between stabilizer and graphene. Nevertheless, most researchers used the toxic reducing agents for the chemical reduction of GO with high efficiency. Moreover, there are few reports on the preparation of water-redispersible graphene powder, which could greatly promote the practical applications of graphene.

On the other hand, the higher aspect ratio and lower density of graphene initiated its application as a corrosion barrier.[17−19] Yet et al. used polyaniline (PANI) chains covalently grafted onto the surfaces of graphene by oxidation polymerization to prepare PANI/graphene composites for corrosion protection of carbon steel. The as-prepared coatings exhibited outstanding barrier properties against O_2 and H_2O compared with neat PANI.[17] Yu et al. reported that the chemical bonding of vinyl-grafted GO and styrene monomer by in situ miniemulsion polymerization enhanced the dispersion of GO in the polystyrene (PS) matrix.[18] The obtained nanocomposites with 2 wt % GO exhibited excellent anticorrosive properties compared with pure PS, and their corrosion protection efficiency increased to 99.53%. However, these chemical modification methods are complicated and difficult to employ in industry. Therefore, simply dispersing graphene into polymer

Received: February 10, 2015
Accepted: July 17, 2015
Published: July 17, 2015

DOI: 10.1021/acsami.5b05531
ACS Appl. Mater. Interfaces 2015, 7, 17641−17648

coatings for corrosion protection would have great advantages in anticorrosion application, and deserve to be developed.

In this study, we demonstrated the utilization of aniline trimer derivative as a stabilizer to disperse commercial graphene in water and then prepared waterborne graphene/epoxy composite coatings. Aniline trimer derivative was used as graphene dispersing agent based on following considerations. First, the conjugate structure of aniline trimer facilitates the dispersion of graphene in solvent through $\pi-\pi$ interactions. Second, aniline trimer displays excellent solvent solubility while maintaining anticorrosive properties similar to those of PANIs. Therefore, this synergistic effect between aniline trimer and graphene is assumed to facilitate the dispersion of graphene and enhancement of the anticorrosion property of epoxy coatings. As a result, the stable aqueous graphene dispersion at high concentration (>1 mg/mL) was prepared directly from commercial graphene without using toxic chemical agents that are essential in conventional preparation methods of aqueous graphene dispersions. Introducting aniline trimer derivative also allowed for the preparation of water-redispersible graphene powder using freeze-drying technology. Furthermore, the resulting aniline trimer derivative-modified graphene exhibited high conductivity (~1.5 S/cm), good electroactivity, and improved electrochemical stability. Adding well-dispersed graphene into waterborne epoxy remarkably improved corrosion protection compared with pure waterborne epoxy coating.

2. EXPERIMENTAL SECTION

2.1. Materials. Aniline, *p*-phenylenediamine sulfate, ammonium persulfate, succinic anhydride, petroleum ether, tetrahydrofuran (THF), ammonium hydroxide, and concentrated HCl were purchased from Aladdin Industrial Corporation, and were used as received without further purification. Graphene slurry (see Table S1 and Figures S1–S3) was supplied by Ningbo Morsh Technology. Co., Ltd. Waterborne epoxy resin (E51) and curing agent (H228B, polyether modified epoxy-amine adduct) were provided by Northwest Yongxin Paint & Coatings Co., Ltd. The Q235 steel electrode was selected for anticorrosion test. The electrode surface was gradually polished with 800 and 1500 SiC abrasive paper, then rinsed with distilled water, degreased by ultrasonication in acetone and finally dried in air.

2.2. Synthesis of Aniline Trimer (AT). The aniline trimer was synthesized according to the literature.[20] Aniline (1.853 g, 20 mmol) and *p*-phenylenediamine sulfate (2.956 g, 10 mmol) were dissolved in 1.0 M HCl solution (150 mL) in an ice–salt bath at −5 °C. Ammonium persulfate (4.541 g, 20 mmol) in 1.0 M HCl solution (50 mL) was dropped into the above-mentioned solution for 1 h. The reaction was continued in air for another 1 h, then filtered to collect the aniline trimer. The cake was washed with 1.0 M HCl solution (200 mL) precooled to 0 °C, and then dedoped in 1.0 M NH_4OH (200 mL) for 2 h. The cake was filtered and washed with water three times. Finally, the aniline trimer was dried at 60 °C in vacuum until constant weight. Yield: 74%. ^{1}H NMR (400 MHz, DMSO-d_6): δ 7.0, 6.8, 6.6 (m, 12 H from benzenoid and quinoid ring), δ 5.4 (s, 4H, $-NH_2$).

2.3. Synthesis of Carboxylated Aniline Trimer (CAT). Aniline trimer (1.24 g, 4.27 mmol) and succinic anhydride (1.04 g, 10 mmol) were dissolved in 40 mL THF with vigorous stirring at 40 °C. The reaction was carried out for 5 h. Subsequently, petroleum ether (200 mL) was dropped into the reaction mixture, and then filtered to collect the solid. Further purification was accomplished by dissolution–precipitation from THF/petroleum ether, and dried at 60 °C in vacuum. Yield: 95%. ^{1}H NMR (400 MHz, DMSO-d_6): δ 10.0 (s, 2H, −COOH), δ 9.7 (s, 2H, −NHCO−), δ 7.6, 7.4, 6.8 (m, 12 H from benzenoid and quinoid ring), δ 2.6 (s, 8H, $-CH_2CH_2-$).

2.4. Preparation of (G-CAT$^-$) Hybrids of G and CAT$^-$. G-CAT$^-$ hybrids were prepared by CAT-assisted dispersion of graphene sheets in aqueous medial. Typically, CAT (0.49 g, 1 mmol) and NaOH (0.08 g, 2 mmol) were added to 95 mL water and then sonicated (200 W) for 60 min to yield a homogeneous CAT$^-$ solution. After that, 5 g of graphene slurry was added into the as-prepared CAT$^-$ solution and then sonicated for 120 min to obtain a G-CAT$^-$ hybrid dispersion.

2.5. Preparation of Waterborne G-CAT$^-$ Anticorrosion Coatings. Five mL of G-CAT$^-$ hybrids aqueous dispersion (5 mg/mL) was added to waterborne curing agent (10 g). After being carefully stirred for 10 min, epoxy resin (5 g) was added. The mixture was stirred for another 10 min, then coated on the Q235 steel electrode with a bar coater, and dried at 25 °C for 48 h. The coating thickness was 20 ± 2 μm measured using a PosiTector6000FNS1 apparatus. For comparison purposes, the pure epoxy coating was prepared in a similar way to G-CAT$^-$/epoxy coating except the addition of G-CAT$^-$.

2.6. Characterizations. ^{1}H NMR spectra were obtained at room temperature on a 400 MHz AVANCE III NMR spectrometer in DMSO-d_6. UV–vis spectra were recorded using a Lambda 950 UV–vis spectrometer. Raman spectra were measured with a confocal Renishaw invia Reflex Raman spectrometer using the wavelength of 632.8 nm. Tapping mode atomic force microscopy (AFM) was performed on a Dimension 3100 V scanning probe microscope. The AFM sample was prepared by dropcasting the G-CAT$^-$ dispersion on new cleaved mica surfaces. The morphology of the coatings was examined using a FEI Quanta FEG 250 scanning electron microscope (SEM). Transmission electron microscopy (TEM) images were obtained on a JEOL JEM2100 TEM instrument operated under a 200 keV acceleration voltage. The electrical conductivity of the G-CAT$^-$ hybrid was measured on a cresbox four-probe meter at room temperature.

Electrochemical corrosion test was performed on CHI-660E electrochemical workstation interfaced to a PC computer. The electrochemical impedance spectroscopy (EIS) and potentiodynamic polarization curves were acquired in 3.5% NaCl solution using classical three-electrode system at room temperature. A saturated calomel electrode (SCE) with a Luggin capillary reference electrode, a platinum plate of 2.5 cm^2 counter electrode and coating/Q235 steel working electrode were used. All the potentials in this paper are reported in the SCE scale. Before measurement, the coating/Q235 steel specimen were initially kept at an open circuit potential (OCP) for 0.5 h. For EIS measurement, the frequency range was 1×10^5 to 1×10^{-2} Hz and the sinusoidal voltage signal amplitude was 20 mV (during 2.5 h immersion, 50 mV amplitude was used). Corrosion parameters from EIS data were fitted using ZsimpWin 3.21 software. Polarization curves were performed with 0.5 mV/s scan rate and started from a potential of −200 mV to +200 mV vs OCP. Cyclic voltammetry were measured in 1 M HCl solution at a scan rate of 20 mV/s.

3. RESULTS AND DISCUSSION

3.1. Fabrication and Characterization of Water-Dispersible Graphene Stabilized by CAT$^-$. The inherent agglomerates of the commercial graphene powder (or slurry) severely limit its practical applications. Therefore, dispersing the aggregated graphene power in various solvents is of crucial importance and expected to provide guidance for other graphene materials. In this work, we prepared aqueous dispersions of graphene nanosheets using a water-soluble CAT derivative (CAT$^-$) as a stabilizer (Figure 1b). The dispersion was stable and no obvious precipitation was observed after 1 day of storage. However, direct dispersion of graphene in water without stabilizers results in agglomerates and precipitation (Figure 1a). The conductivity of the CAT$^-$-modified graphene (G-CAT$^-$, ~ 1 mg CAT$^-$ on 1 mg garphene) composite was measured to be ~1.5 S/cm, almost 4 times of magnitude larger than that of sulfonated polyaniline-modified graphene (SPANI/r-G) composite film prepared by the same procedure.[13] This may be due to the high conductivity

DOI: 10.1021/acsami.5b05531
ACS Appl. Mater. Interfaces 2015, 7, 17641–17648

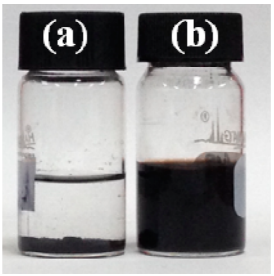

Figure 1. Digital images of water dispersions (1 mg/mL) of (a) graphene and (b) CAT^--functionalized graphene.

of CAT^- that was not reduced during the preparation of G-CAT^- hybrid, whereas SPANI component was reduced by hydrazine in preparing SPANI/r-G, resulting in relatively low conductivity.[13] More importantly, the introduction of CAT^- also allowed for the preparation of water-redispersible graphene powder using freeze-drying technology, which could greatly promote the practical applications of graphene.

To study the interaction between CAT^- and graphene sheets, we studied the CAT^--functionalized graphene (G-CAT^- hybrid) by Raman and UV−vis spectra. Figure 2 shows the Raman spectra of graphene, CAT^- and G-CAT^- hybrid. The graphene exhibits a G band at 1582 cm^{-1} and a D band at 1345 cm^{-1} (Figure 2a). The G band corresponds to the in-plane bonding stretching motion of C sp^2 atoms, whereas the D band represents the breaking mode near the K zone boundary.[21,22] For CAT^-, there are 1342 cm^{-1} band assigning to C−$N^{+\cdot}$ stretching, 1490 cm^{-1} band due to C═N stretching of the quinoid units and 1603 cm^{-1} band representing C═C stretching of the quinoid units, all of which reveal the structure of CAT^- (Figure 2b).[23] The G band was red-shifted from 1582 cm^{-1} for graphene to 1579 cm^{-1} for G-CAT^- hybrid, indicating that a charge transfer exists between graphene and CAT^-.[24,25] Furthermore, compared with CAT^-, the G-CAT^- hybrid shows a blue shift of the C−$N^{+\cdot}$ stretching resulting from the $\pi-\pi$ interaction between graphene and CAT^-.[26]

UV−vis spectra of CAT^- and G-CAT^- hybrid supernatants are shown in Figure 3. The two absorption peaks at 307 and 468 nm appearing in CAT^- spectrum are attributed to $\pi-\pi^*$ transition of benzene unit and π_B-π_Q transition of benzenoid (B) to quinoid (Q).[27] The G-CAT^- hybrid shows two absorption peaks at 311 and 474 nm similar to CAT^-. However, the Q/B intensity ratio of the G-CAT^- hybrid

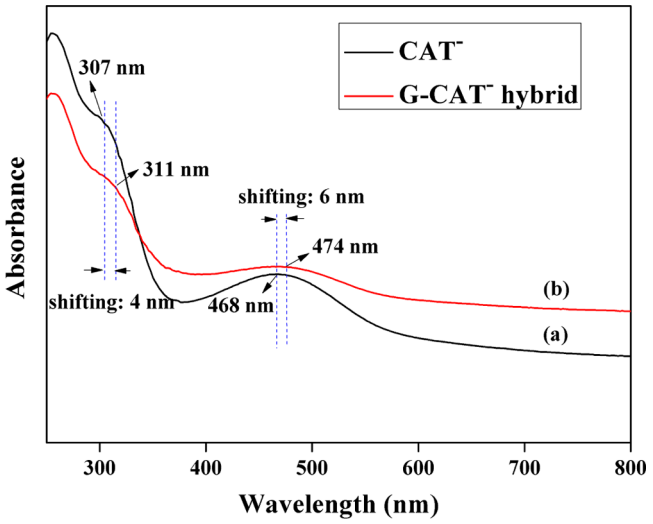

Figure 3. UV−vis spectra of (a) CAT^- and (b) G-CAT^- hybrid suspension.

increased along with a slight red shift, which indicates the $\pi-\pi$ interaction between graphene and CAT^-.

Direct evidence for the dispersion state of graphene sheets with CAT^- in water can be further obtained by AFM and TEM observation. Figure 4 displays a typical AFM image of G-CAT^- hybrid. From the AFM photo, it can be observed that the average thickness of G-CAT^- sheets was ~2.5 nm, which indicates that the graphene nanosheets were almost exfoliated. The nanolayer was thicker than the single graphene sheet, possibly due to the multilayer adsorption of CAT^- chains on the surface of graphene.[13] The thickness of graphene without CAT^- was also determined by AFM to be about 10 nm (see Figure S3). Figure 5 displays a typical TEM photo of G-CAT^- hybrid, which looks like a transparent thin film with wrinkled surfaces. The above results also demonstrated that the agglomeration of the commercial graphene in water can be prevented by the anchored CAT^- chains.

3.2. Electroactive Properties of G-CAT^- Hybrids. As is well-known, oligoanilines have good electroactivity similar to that of PANI.[28] Cyclic voltammetry (CV) was used to examine the electrochemical property of the G-CAT^- hybrids. The G-CAT^- hybrid and CAT^- modified electrodes were prepared by depositing the corresponding aqueous dispersion or solution on glassy carbon electrodes and drying at room temperature, and

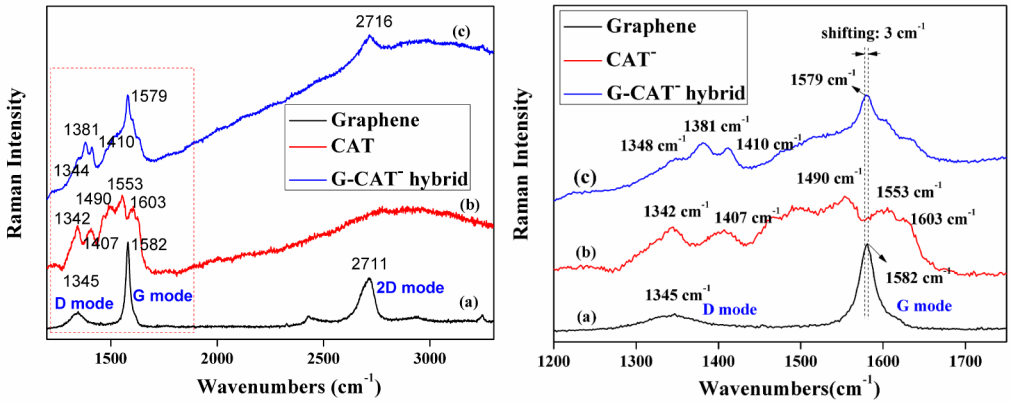

Figure 2. Raman spectra of (a) graphene, (b) CAT^-, and (c) G-CAT^- hybrid.

DOI: 10.1021/acsami.5b05531
ACS Appl. Mater. Interfaces 2015, 7, 17641−17648

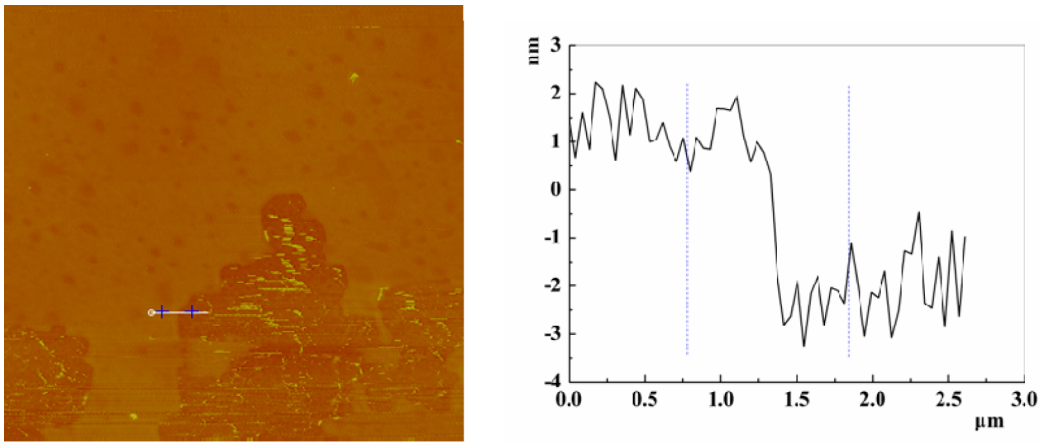

Figure 4. Typical AFM image of G-CAT$^-$ hybrid.

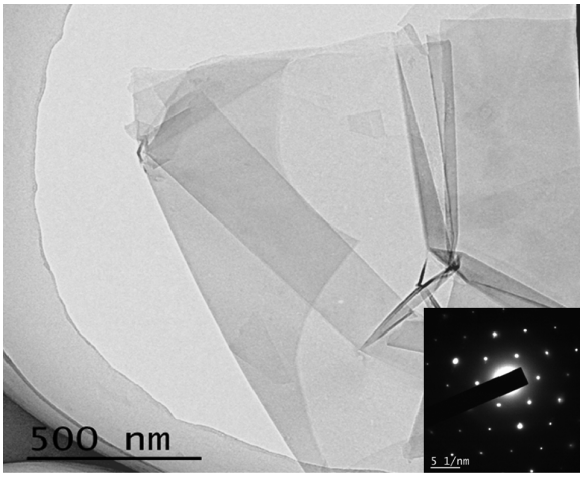

Figure 5. Typical TEM image of G-CAT$^-$ hybrid.

Scheme 1. Molecular Structure of CAT$^-$ in Various Oxidation States

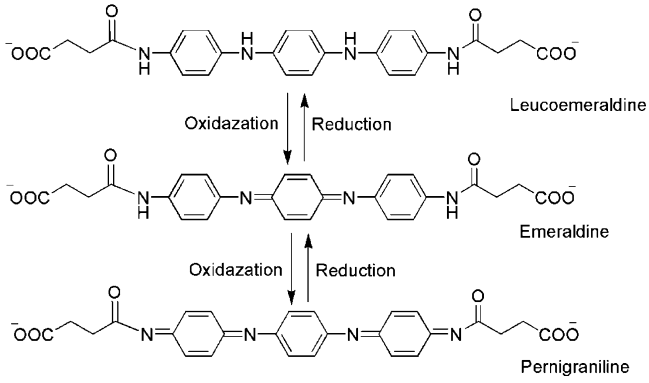

the CV curves of these electrodes were measured in 1.0 M HCl solution, as shown in Figure 6. The G-CAT$^-$ hybrid exhibits two pairs of oxidation/reduction peaks at 0.301 and 0.550 V (Figure 6B), which could be ascribed to the transition from a leucoemeraldine base (LEB) to an emeraldine base (EB) and further to a pernigraniline base (PB), respectively (Scheme 1).[27] Only one redox peak at 0.517 V was observed for the CAT$^-$ modified electrode (Figure 6A), which can be assigned to the LEB to EB transition.

It is worth noting that the CV current of G-CAT$^-$ hybrid modified electrode are much higher than that of CAT$^-$ modified electrode in HCl aqueous solution. Similar phenomenon was also observed in organic solution, as shown in Figure S5. This could be ascribed to the higher conductivity of graphenen. Moreover, the dissolution of CAT$^-$ from the electrode surface could be clearly seen when the CAT$^-$ modified electrode was immersed in HCl aqueous solution. The addition of graphene nanosheets was found to largely improve the film-forming property and water resistance of CAT$^-$, which may be attributed to the strong $\pi-\pi$ interactions between CAT$^-$ and graphene.[13] Compared with pure CAT$^-$,

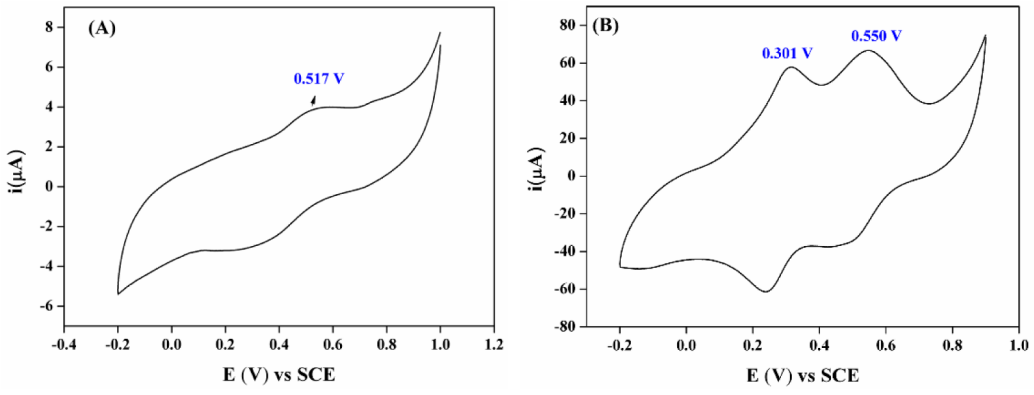

Figure 6. Cyclic voltammograms of (A) CAT$^-$ and (B) G-CAT$^-$ hybrid modified electrodes in 1.0 M HCl solution.

DOI: 10.1021/acsami.5b05531
ACS Appl. Mater. Interfaces 2015, 7, 17641−17648

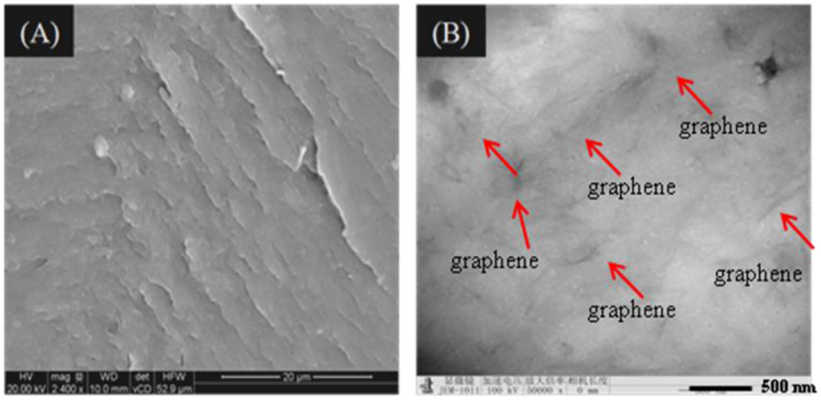

Figure 7. (A) SEM and (B) TEM micrographs of the G-CAT$^-$/epoxy coating containing 0.5 wt % of G-CAT$^-$ hybrid.

the improved water resistance of the G-CAT$^-$ hybrid makes it more suitable as a corrosion inhibitor in waterborne coatings, as discussed in the following sections.

3.3. Preparation and Morphologies of G-CAT$^-$/Epoxy Coatings. G-CAT$^-$/epoxy coatings were prepared by a curing reaction of epoxy resin with waterborne curing agent containing G-CAT$^-$ hybrid. The G-CAT$^-$/curing agent dispersed in water was stable and no precipitation was seen after storing for one month. To further study the dispersion capability of graphene nanosheets in polymer matrix, we determined the morphologies of the G-CAT$^-$/epoxy coating by SEM and TEM. Figure 7 gives the SEM image of the fracture surface of the G-CAT$^-$/epoxy coating with 0.5 wt % G-CAT$^-$ hybrid. The G-CAT$^-$/epoxy coating exhibited rough fracture surfaces. Moreover, the CAT$^-$-modified graphene showed two-dimensional parallel alignment in the epoxy matrix, which would provide the enhanced barrier properties of epoxy coating. The TEM image in Figure 7 displayed the garphene nanoscopic dispersion in the G-CAT$^-$/epoxy coating. The black lines represented individual graphene sheets, whereas the bright areas represented the epoxy matrix. It is revealed that CAT$^-$-functionalized graphene nanosheets were well-dispersed in epoxy coatings.

3.4. Anticorrosion Properties of Waterborne G-CAT$^-$/epoxy coatings. Potentiodynamic polarization curves and EIS were employed to study the anticorrosive behaviors of the G-CAT$^-$/epoxy coating. Figure 8 shows the corrosion protection behavior of bare Q235, pure epoxy and G-CAT$^-$ (0.5 wt %)/epoxy-coated Q235 steel in 3.5% NaCl solution under potentiodynamic polarization conditions. The polarization curves displayed a reasonable linear Tafel region in both anodic and cathodic branches. Therefore, the kinetic parameters including corrosion potential (E_{corr}), corrosion density (i_{corr}), anodic Tafel slope (b_a), and cathodic Tafel slope (b_c) were determined and summarized in Table 1. The values of protection efficiency from i_{corr} were calculated by the following equation,[20,29] where i_{corr} (uncoated) and i_{corr} (coated) are the uncoated and coated specimen corrosion current densities, respectively.

$$P_{EF}\% = \frac{i_{corr}(\text{uncoated}) - i(\text{coated})}{i_{corr}(\text{uncoated})} 100\%$$

Generally, a higher E_{corr} and a lower i_{corr} indicate better corrosion protection. The E_{corr} of the G-CAT$^-$/epoxy-coated Q235 electrode was −0.632 V, which was more positive than pure epoxy-coated (−0.681 V) and bare Q235 steel (−0.693 V). Moreover, the i_{corr} value of the G-CAT$^-$/epoxy-coated

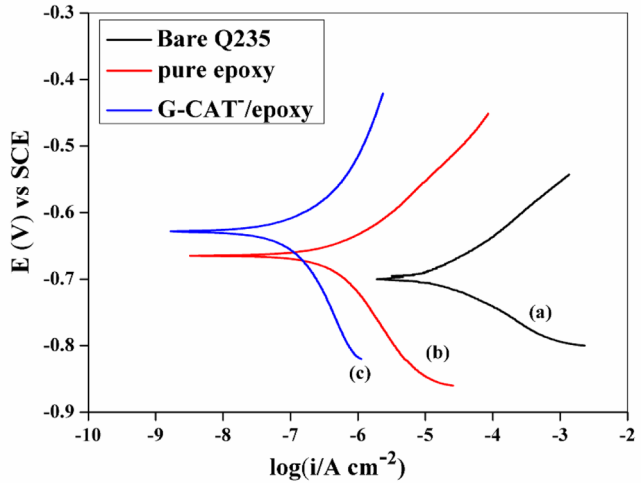

Figure 8. Polarization curves of (a) bare, (b) pure epoxy, and (c) G-CAT$^-$/epoxy-coated Q235 steel electrodes immersed in 3.5% NaCl solution after 96 h.

Q235 electrode (0.145 μA cm^{-2}) was much lower than that of pure epoxy-coated (0.562 μA cm^{-2}) and bare Q235 steel (17.1 μA cm^{-2}). The P_{EF}% of the G-CAT$^-$/epoxy coating (99.2%) was higher than that of pure epoxy coating (96.7%). Yet et al. has reported that graphene-based epoxy composites displayed outstanding barrier properties against O_2 and H_2O.[17] Therefore, the enhanced anticorrosive performance of the G-CAT$^-$/epoxy coated on Q235 steel might be due to the well-dispersed graphene in the coating that increases the tortuosity of the diffusion path for O_2 and H_2O molecules.[17]

EIS was further used to investigate corrosion protection mechanism of the G-CAT$^-$/epoxy composites, as shown in Figure 9. For pure epoxy coating, the radius of two capacitive arcs in the middle-low and high frequency region decreased with immersion time. It is important to note that the impedance modulus of G-CAT$^-$/epoxy coating first decreased during initial immersion times (from 2.5 to 24 h), then increased to some extent and remained stable (form 24 to 96 h). The presence of graphene as filler gives mechanical integrity to the epoxy coating in corrosive media. This composite coating acts as barrier and inhibits the ingress of corrosive ions through them. The impedance modulus $|Z|_{0.01\ Hz}$ can characterize the corrosion protection of coating/metal system, which is in inverse proportion to corrosion rate.[30] The $|Z|_{0.01\ Hz}$ of the G-CAT$^-$/epoxy-coated Q235 electrode was about one order

DOI: 10.1021/acsami.5b05531
ACS Appl. Mater. Interfaces 2015, 7, 17641−17648

Table 1. Corrosion Parameters of Bare Q235, Pure Epoxy, and G-CAT$^-$/Epoxy-Coated Q235 Steel Electrodes Immersed in 3.5% NaCl Solution after 96 h

	E_{corr} (V), vs SCE	i_{corr} (μA cm^{-2})	b_a (mV dec^{-1})	b_c (mV dec^{-1})	thickness (μm)	P_{EF} (%)
bare Q235[a]	−0.693	17.1	72.8	60.2		
pure epoxy	−0.681	0.562	103.1	145.4	20 ± 2	96.7
G-CAT$^-$/epoxy[b]	−0.632	0.145	168.1	261.2	20 ± 2	99.2

[a]24 h immersion. [b]0.5 wt % G-CAT$^-$ hybrid in the waterborne epoxy coating.

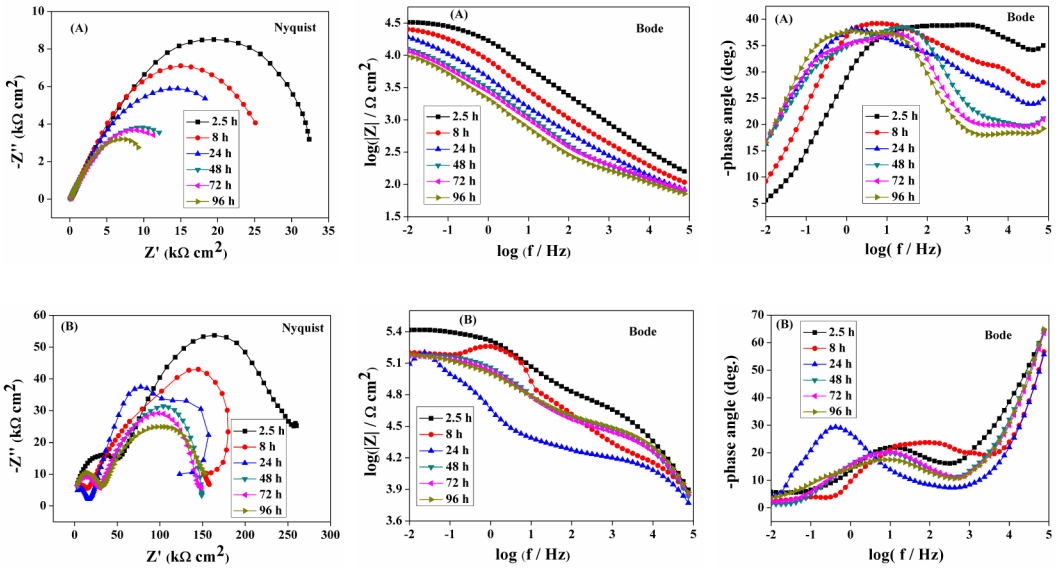

Figure 9. Nyquist and Bode plots of (A) pure epoxy and (B) G-CAT$^-$/epoxy-coated Q235 steel electrodes immersed in 3.5% NaCl solution after different times.

higher than that of pure epoxy coating after 96 h immersion (see Bode plots in Figure 9), indicating that G-CAT$^-$/epoxy coating has better corrosion protection for the Q235 steel than pure epoxy.

For quantitative estimation of the evolution of the anticorrosion properties of the G-CAT$^-$/epoxy composites, EIS data were fitted with an equivalent circuit, as shown in Figure 10 and the fitted corrosion parameters were listed in Table 2.[31] The R_s is the solution resistance, and R_c and R_{ct} represent the coating and charge-transfer resistance, respectively. Q_c and Q_{dl} represent the coating and double-layer capacitance, respectively. A higher R_c implies a smaller number of H_2O and O_2 molecules penetrated into the coatings.[32] R_{ct} is a parameter to characterize the resistance to electron transfer across metal surface and is in inverse proportion to the corrosion rate.[31] It is noted that the R_c and R_{ct} of the G-CAT$^-$/epoxy-coated electrode were much higher than those of epoxy after the same immersion time (see Table 2). It may result from barrier properties of graphene against O_2 and H_2O.[17] The Q_c would increase with the electrolyte solution absorption the in the coating.[33] The Q_c of G-CAT$^-$/epoxy coating changed very little during the whole immersion period, which was much lower than that of pure epoxy after the same immersion time (Figure 11). It indicates that G-CAT$^-$/epoxy coating has an excellent water barrier property.

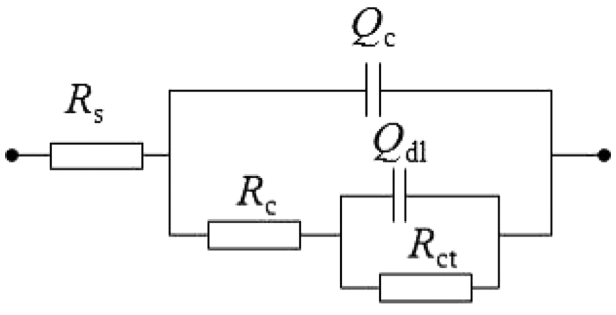

Figure 10. Equivalent circuit used to fit the EIS data.

Moreover, the water diffusion coefficients of metal/coating systems were calculated based on the changes of the coating capacitance. The water diffusion coefficient D could be calculated by means of the simplified Fick's second law of diffusion.[34]

$$\frac{\log Q_c - \log Q_0}{\log Q_\infty - \log Q_0} = \frac{2}{L}\sqrt{\frac{D}{\pi}}\sqrt{t}$$

Where Q_0, Q_c, and Q_∞ are the coating capacitances at the beginning of the immersion time t_0, the time t_c and the time in saturated water absorption state t_∞, respectively. D is the diffusion coefficient, L is the coating thickness. The D of G-CAT$^-$/epoxy coating was calculated to be 1.36×10^{-9} cm^2/s from the logQ_c−$t^{1/2}$ curves (Figure 12), which was about one-fifth of the pure epoxy coating (6.01×10^{-9} cm^2 S^{-1}). It further suggests that G-CAT$^-$/epoxy coating showed better barrier property than pure epoxy coating. Therefore, the enhanced anticorrosion performance of the G-CAT$^-$/epoxy coating can be attributed to barrier properties of graphene.

DOI: 10.1021/acsami.5b05531
ACS Appl. Mater. Interfaces 2015, 7, 17641−17648

Table 2. Electrochemical Corrosion Parameters Fitted from the Equivalent Circuit

	time (h)	R_s (Ω cm^2)	Q_c (μF cm^{-2})	n_1	R_c (KΩ cm^2)	Q_{dl} (μF cm^{-2})	n_2	R_{ct} (KΩ cm^2)
pure epoxy	2	0.01	12.7	0.51	4.87	3.71	0.62	32.6
	8	0.01	21.2	0.51	0.839	18.9	0.55	31.1
	24	0.01	39.3	0.57	0.421	21.3	0.59	29.1
	48	0.01	101	0.62	0.251	29.1	0.63	23.5
	72	0.01	114	0.56	0.273	43.5	0.61	23.3
	96	0.01	126	0.61	0.173	112	0.56	16.2
G-CA$^-$/epoxy[a]	2	0.01	0.0089	0.73	46.3	1.031	0.54	232
	8	0.01	0.0121	0.83	16.8	0.733	0.59	183
	24	0.01	0.0264	0.72	17.2	8.43	0.61	153
	48	0.01	0.0633	0.76	29.2	1.87	0.57	128
	72	0.01	0.423	0.79	26.4	2.17	0.54	129
	96	0.01	0.571	0.83	27.2	3.45	0.55	104

[a]0.5 wt % G-CAT$^-$ hybrid in the waterborne epoxy coating.

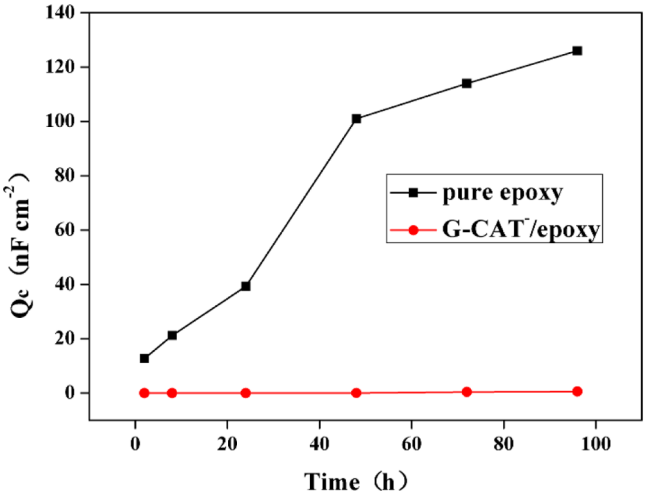

Figure 11. Time dependence of the coating capacitance (Q_c) of different composite coatings immersed in 3.5% NaCl solution.

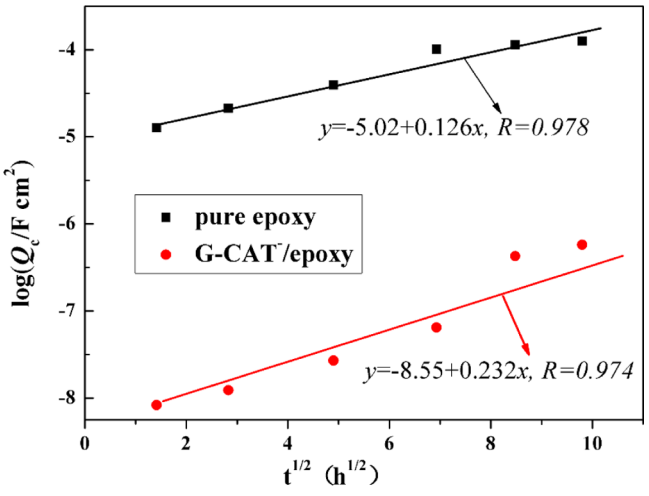

Figure 12. logQ_c–$t^{1/2}$ curves of different composite coatings immersed in 3.5% NaCl solution.

4. CONCLUSIONS

We synthesized CAT by reaction of aniline trimer with succinic anhydride, and demonstrated the feasibility of CAT derivative as a stabilizer to disperse commercial graphene in water. The graphene aqueous dispersion at high concentration (>1 mg/mL) was obtained with high stability due to strong π–π interactions between CAT$^-$ and graphene. Moreover, the CAT$^-$-functionalized graphene sheets exhibited high conductivity (~1.5 S/cm), good electroactivity and electrochemical stability. The addition of well-dispersed graphene into waterborne epoxy remarkably improved corrosion protection compared with pure waterborne epoxy coating, which may be due to the improved water barrier properties from G-CAT$^-$/epoxy coating.

■ ASSOCIATED CONTENT

Supporting Information

The Supporting Information is available free of charge on the ACS Publications website at DOI: 10.1021/acsami.5b05531.

Characterization of commercial graphene and carboxylated aniline trimer (CAT) (PDF)

■ AUTHOR INFORMATION

Corresponding Authors

*E-mail: liushuan@nimte.ac.cn. Tel.: +86 0574 87911126.

*E-mail: zhaohaichao@nimte.ac.cn.

Notes

The authors declare no competing financial interest.

■ ACKNOWLEDGMENTS

The research is financially supported by the Ningbo Natural Science Foundation (2015A610016), National Natural Science Foundation of China (21404112), and China Postdoctoral Science Foundation (2014M561798). The authors appreciate Dr. Qing-Yun Wu in Ningbo University for her discussion and suggestion.

■ REFERENCES

(1) Robinson, J. T.; Perkins, F. K.; Snow, E. S.; Wei, Z.; Sheehan, P. E. Reduced Graphene Oxide Molecular Sensors. *Nano Lett.* **2008**, *8* (10), 3137–3140.

(2) Yoonessi, M.; Shi, Y.; Scheiman, D. A.; Lebron-Colon, M.; Tigelaar, D. M.; Weiss, R. A.; Meador, M. A. Graphene Polyimide Nanocomposites; Thermal, Mechanical, and High-Temperature Shape Memory Effects. *ACS Nano* **2012**, *6* (9), 7644–7655.

(3) Dimitrakakis, G. K.; Tylianakis, E.; Froudakis, G. E. Pillared Graphene: A New 3-D Network Nanostructure for Enhanced Hydrogen Storage. *Nano Lett.* **2008**, *8* (10), 3166–3170.

(4) Hsieh, Y.-P.; Hofmann, M.; Chang, K.-W.; Jhu, J. G.; Li, Y.-Y.; Chen, K. Y.; Yang, C. C.; Chang, W.-S.; Chen, L.-C. Complete

DOI: 10.1021/acsami.5b05531
ACS Appl. Mater. Interfaces 2015, 7, 17641–17648

Corrosion Inhibition through Graphene Defect Passivation. *ACS Nano* **2014**, *8* (1), 443−448.
(5) McAllister, M. J.; Li, J.-L.; Adamson, D. H.; Schniepp, H. C.; Abdala, A. A.; Liu, J.; Herrera-Alonso, M.; Milius, D. L.; Car, R.; Prud'homme, R. K.; Aksay, I. A. Single Sheet Functionalized Graphene by Oxidation and Thermal Expansion of Graphite. *Chem. Mater.* **2007**, *19* (18), 4396−4404.
(6) Paton, K. R.; Varrla, E.; Backes, C.; Smith, R. J.; Khan, U.; O'Neill, A.; Boland, C.; Lotya, M.; Istrate, O. M.; King, P.; Higgins, T.; Barwich, S.; May, P.; Puczkarski, P.; Ahmed, I.; Moebius, M.; Pettersson, H.; Long, E.; Coelho, J.; O'Brien, S. E.; McGuire, E. K.; Sanchez, B. M.; Duesberg, G. S.; McEvoy, N.; Pennycook, T. J.; Downing, C.; Crossley, A.; Nicolosi, V.; Coleman, J. N. Scalable production of large quantities of defect-free few-layer graphene by shear exfoliation in liquids. *Nat. Mater.* **2014**, *13* (6), 624−630.
(7) He, P.; Sun, J.; Tian, S.; Yang, S.; Ding, S.; Ding, G.; Xie, X.; Jiang, M. Processable Aqueous Dispersions of Graphene Stabilized by Graphene Quantum Dots. *Chem. Mater.* **2015**, *27* (1), 218−226.
(8) Zhang, C.; Huang, S.; Tjiu, W. W.; Fan, W.; Liu, T. Facile Preparation of Water-dispersible Graphene Sheets Stabilized by Acid-treated Multi-walled Carbon Nanotubes and their Poly(vinyl alcohol) Composites. *J. Mater. Chem.* **2012**, *22* (6), 2427−2434.
(9) Eigler, S.; Hirsch, A. Chemistry with Graphene and Graphene Oxide-Challenges for Synthetic Chemists. *Angew. Chem., Int. Ed.* **2014**, *53* (30), 7720−7738.
(10) Li, D.; Muller, M. B.; Gilje, S.; Kaner, R. B.; Wallace, G. G. Processable Aqueous Dispersions of Graphene Nanosheets. *Nat. Nanotechnol.* **2008**, *3* (2), 101−105.
(11) Si, Y.; Samulski, E. T. Synthesis of Water Soluble Graphene. *Nano Lett.* **2008**, *8* (6), 1679−1682.
(12) Teng, C.-C.; Ma, C.-C. M.; Lu, C.-H.; Yang, S.-Y.; Lee, S.-H.; Hsiao, M.-C.; Yen, M.-Y.; Chiou, K.-C.; Lee, T.-M. Thermal Conductivity and Structure of Non-covalent Functionalized Graphene/Epoxy Composites. *Carbon* **2011**, *49* (15), 5107−5116.
(13) Bai, H.; Xu, Y.; Zhao, L.; Li, C.; Shi, G. Non-covalent Functionalization of Graphene Sheets by Sulfonated Polyaniline. *Chem. Commun.* **2009**, *13*, 1667.
(14) Cao, L.; Liu, X.; Na, H.; Wu, Y.; Zheng, W.; Zhu, J. How a Bio-based Epoxy Monomer Enhanced the Properties of Diglycidyl Ether of Bisphenol A (DGEBA)/Graphene Composites. *J. Mater. Chem. A* **2013**, *1* (16), 5081−5088.
(15) Xu, Y.; Bai, H.; Lu, G.; Li, C.; Shi, G. Flexible Graphene Films via the Filtration of Water-Soluble Noncovalent Functionalized Graphene Sheets. *J. Am. Chem. Soc.* **2008**, *130* (18), 5856−5857.
(16) Stankovich, S.; Piner, R. D.; Chen, X.; Wu, N.; Nguyen, S. T.; Ruoff, R. S. Stable Aqueous Dispersions of Graphitic Nanoplatelets via the Reduction of Exfoliated Graphite Oxide in the Presence of Poly(sodium 4-styrenesulfonate). *J. Mater. Chem.* **2006**, *16* (2), 155−158.
(17) Chang, C. H.; Huang, T. C.; Peng, C. W.; Yeh, T. C.; Lu, H. I.; Hung, W. I.; Weng, C. J.; Yang, T. I.; Yeh, J. M. Novel Anticorrosion Coatings Prepared from Polyaniline/Graphene Composites. *Carbon* **2012**, *50* (14), 5044−5051.
(18) Yu, Y.-H.; Lin, Y.-Y.; Lin, C.-H.; Chan, C.-C.; Huang, Y.-C. High-performance Polystyrene/Graphene-based Nanocomposites with Excellent Anti-corrosion Properties. *Polym. Chem.* **2014**, *5* (2), 535−550.
(19) Chang, K.-C.; Ji, W.-F.; Lai, M.-C.; Hsiao, Y.-R.; Hsu, C.-H.; Chuang, T.-L.; Wei, Y.; Yeh, J.-M.; Liu, W.-R. Synergistic Effects of Hydrophobicity and Gas Barrier Properties on the Anticorrosion Property of PMMA Nanocomposite Coatings Embedded with Graphene Nanosheets. *Polym. Chem.* **2014**, *5* (3), 1049−1056.
(20) Weng, C.-J.; Chang, C.-H.; Peng, C.-W.; Chen, S.-W.; Yeh, J.-M.; Hsu, C.-L.; Wei, Y. Advanced Anticorrosive Coatings Prepared from the Mimicked Xanthosoma Sagittifolium-leaf-like Electroactive Epoxy with Synergistic Effects of Superhydrophobicity and Redox Catalytic Capability. *Chem. Mater.* **2011**, *23* (8), 2075−2083.
(21) Ferrari, A. C.; Robertson, J. Interpretation of Raman Spectra of Disordered and Amorphous Carbon. *Phys. Rev. B: Condens. Matter Mater. Phys.* **2000**, *61* (20), 14095−14107.
(22) Cancado, L. G.; Pimenta, M. A.; Neves, B. R. A.; Dantas, M. S. S.; Jorio, A. Influence of the Atomic Structure on the Raman Spectra of Graphite Edges. *Phys. Rev. Lett.* **2004**, *93* (24), 247401.
(23) Trchová, M.; Morávková, Z.; Bláha, M.; Stejskal, J. Raman Spectroscopy of Polyaniline and Oligoaniline Thin Films. *Electrochim. Acta* **2014**, *122* (0), 28−38.
(24) Lei, Y.; Tang, Z.; Liao, R.; Guo, B. Hydrolysable Tannin as Environmentally Friendly Reducer and Stabilizer for Graphene Oxide. *Green Chem.* **2011**, *13* (7), 1655−1658.
(25) Liang, Y.; Wu, D.; Feng, X.; Müllen, K. Dispersion of Graphene Sheets in Organic Solvent Supported by Ionic Interactions. *Adv. Mater.* **2009**, *21* (17), 1679−1683.
(26) Yan, J.; Wei, T.; Shao, B.; Fan, Z.; Qian, W.; Zhang, M.; Wei, F. Preparation of a Graphene Nanosheet/Polyaniline Composite with High Specific Capacitance. *Carbon* **2010**, *48* (2), 487−493.
(27) Guo, B. L.; Finne-Wistrand, A.; Albertsson, A. C. Molecular Architecture of Electroactive and Biodegradable Copolymers Composed of Polylactide and Carboxyl-Capped Aniline Trimer. *Biomacromolecules* **2010**, *11* (4), 855−863.
(28) Yang, T. I.; Peng, C. W.; Lin, Y. L.; Weng, C. J.; Edgington, G.; Mylonakis, A.; Huang, T. C.; Hsu, C. H.; Yeh, J. M.; Wei, Y. Synergistic Effect of Electroactivity and Hydrophobicity on the Anticorrosion Property of Room-temperature-cured Epoxy Coatings with Multi-scale Structures Mimicking the Surface of Xanthosoma Sagittifolium Leaf. *J. Mater. Chem.* **2012**, *22* (31), 15845−15852.
(29) Gu, L.; Liu, S.; Zhao, H.; Yu, H. Anticorrosive Oligoaniline-containing Electroactive Siliceous Hybrid Materials. *RSC Adv.* **2015**, *5* (69), 56011−56019.
(30) Hang, T. T. X.; Truc, T. A.; Duong, N. T.; Pébère, N.; Olivier, M.-G. Layered Double Hydroxides as Containers of Inhibitors in Organic Coatings for Corrosion Protection of Carbon Steel. *Prog. Org. Coat.* **2012**, *74* (2), 343−348.
(31) Wei, H.; Ding, D.; Wei, S.; Guo, Z. Anticorrosive Conductive Polyurethane Multiwalled Carbon Nanotube Nanocomposites. *J. Mater. Chem. A* **2013**, *1* (36), 10805−10813.
(32) Zhang, Y.; Shao, Y.; Zhang, T.; Meng, G.; Wang, F. High Corrosion Protection of a Polyaniline/Organophilic Montmorillonite Coating for Magnesium Alloys. *Prog. Org. Coat.* **2013**, *76* (5), 804−811.
(33) Yu, M.; Yuan, W.; Li, C.; Hong, J.-D.; Shi, G. Performance Enhancement of a Graphene-sulfur Composite as a Lithium-sulfur Battery Electrode by Coating with an Ultrathin Al2O3 film via Atomic Layer Deposition. *J. Mater. Chem. A* **2014**, *2* (20), 7360−7366.
(34) Wind, M. M.; Lenderink, H. J. W. A Capacitance Study of Pseudo-fickian Diffusion in Glassy Polymer Coatings. *Prog. Org. Coat.* **1996**, *28* (4), 239−250.

DOI: 10.1021/acsami.5b05531
ACS Appl. Mater. Interfaces 2015, 7, 17641−17648